Balmer, R. S., Friel, I., Hepplestone, S., Isberg, J., Uren, M., Markham, M. L., Palmer, N. L., Pilkington, J., Huggett, P., Majdi, S., & Lang, R. (2013). Transport behavior of holes in boron delta-doped diamond structures. *Journal of Applied Physics*, *113*(3), [033702]. https://doi.org/10.1063/1.4775814

TRANSPORT BEHAVIOR OF HOLES IN BORON DELTA-DOPED DIAMOND STRUCTURES

Richard S Balmer[1,a], Ian Friel[1], Steven Hepplestone[2], Jan Isberg[3], Michael J Uren[5,6], Matthew L Markham[1], Nicola L Palmer[1], James Pilkington[4], Paul Huggett[4], Saman Majdi[3], Richard Lang[5]

[1]Element Six Ltd, Kings Ride Park, Ascot, Berkshire, UK, SL5 8BP

[2]Advanced Technology Institute, University of Surrey, Guildford, Surrey, UK

[3]Division for Electricity Research, Box 534, S-751 21, University of Uppsala, Sweden

[4]INEX, University of Newcastle, Newcastle upon Tyne, UK

[5]Diamond Microwave Devices Ltd, Leeds Innovation Centre, 103 Clarendon Road, Leeds, UK

[6]H H Wills Physics Laboratory, University of Bristol, UK

ABSTRACT

Boron delta-doped diamond structures have been synthesized using microwave plasma chemical vapor deposition, and fabricated into FET and gated Hall bar devices for assessment of the electrical characteristics. A detailed study of variable temperature Hall, conductivity and field-effect mobility measurements was completed. This was supported by Schrödinger-Poisson and relaxation time calculations based upon application of Fermi's golden rule. A two carrier-type model was developed with an activation energy of ~0.2 eV between the delta layer lowest subband with mobility ~1 cm^2/Vs and the bulk valence band with high mobility. This new understanding of the transport of holes in such boron delta-doped structures has shown that although Hall mobility as high as 900 cm^2/Vs was measured at room temperature, this dramatically overstates the actual useful performance of the device.

[a] Corresponding author e-mail: richard.balmer@e6.com

I. INTRODUCTION

Single crystal diamond synthesized by chemical vapor deposition (CVD) has a number of important electrical properties which are attractive for semiconductor devices. The key differentiating properties of single crystal CVD diamond are its wide bandgap of 5.4 eV, its unrivalled room temperature thermal conductivity up to 22 W cm^{-1} K^{-1} [1], its maximum breakdown field strength predicted to be between 10 and 20 MV cm^{-1} [2], [3] and its high intrinsic mobility [4]. Hence, CVD diamond has been researched in depth for device applications aiming to leverage these extreme properties towards higher electrical performance, particularly where physical robustness and tolerance to harsh environmental conditions are required.

An area of intense research is diamond high frequency field effect transistors (FET) for microwave solid state power amplifiers. Although GaN materials and devices are significantly more advanced in their development compared to diamond, diamond may offer performance benefits, however the key is to establish and fabricate suitable device designs which can utilize diamond's extreme properties. As an intrinsic material diamond has exceptional electronic properties, however its close-packed atomic structure and low dielectric constant of 5.7 result in an absence of donors or acceptors that are thermally ionized at room temperature thus placing considerable constraints on possible device configurations. The comparatively high activation energy of dopant impurities precludes a conventional MESFET architecture; hence alternative designs have been explored. One such design is the surface FET which employs a conductive p-channel formed by charge transfer at a surface terminated with hydrogen [5], [6]. This design has achieved highly encouraging RF performance of f_T of 45 GHz, and f_{MAX} of 120 GHz [7], and useful RF power density of 2.1 W/mm [8], [9] although these values are some way short of the GaN competition which has demonstrated f_T and f_{MAX} >300 GHz and output power densities >40 W/mm [10], [11]. There is also concern over the stability of hydrogen terminated surface FETs at the high junction temperatures and drain voltages required for high output power. As such there is also interest in devices

using the more stable oxygen-terminated surface, despite its high interface state density which impacts device performance [12].

Here, we discuss the development of another such approach, namely boron delta-doping. The delta-doped FET design aims to achieve a degree of separation between the charge carriers and ionized impurities by incorporating an ultra-thin 'delta' doped layer, a technique pioneered in silicon devices and commonly used in III-V devices [13]. In diamond, the delta layer is a very thin (ideally a few monolayers) highly boron doped region on the surface of, or buried within 'undoped' intrinsic diamond. The room temperature activation energy of holes for low boron acceptor density in diamond is unacceptably high at 0.37 eV, thus the boron doping density has to be greater than $3 – 4.5\times10^{20}$ cm^{-3} [14], [15] so that it forms a metallic impurity band which overlaps the valence band maximum and the activation energy tends to zero [16]. On the other hand, the total sheet charge density in the delta layer must be low enough that the delta layer can be fully depleted (pinched off) without breakdown by an applied gate field in a FET structure. A practical target for the sheet density giving a combination of high current and gate control is $1–1.5\times10^{13}$ cm^{-2}. Applying these boundary conditions, one can determine that the required delta layer profile with B_{peak} comparable to the metal-insulator transition has thickness <1 nm [17]. It is expected that a percentage of the holes confined in the ground state of the delta layer where the mobility is low due to ionized impurity scattering [16], are either thermally excited into higher energy subbands in the potential well, or ideally into bulk states with very little wavefunction overlap with the doped layer [18]. The expectation is that there will be a direct device benefit from an enhancement in mobility for nanometer thickness delta-layers.

The diamond delta-FET approach has been demonstrated by the University of Ulm [19] with small signal measurements reported of 1 GHz and 3 GHz for f_T and f_{MAX} respectively [20]. However, the current density was limited due to significant parasitic series resistances associated with the access regions, and the low measured mobility of 20-30 cm^2/Vs.

This paper describes the characterization of boron delta-doped structures grown by CVD. A detailed study using variable temperature *I-V* and Hall measurements of delta doped devices is presented. Furthermore, an analytical carrier transport model and a physical model employing 1D Schrödinger-Poisson simulations and 2D scattering calculations have been developed to describe the experimental observations. These have led to a new understanding of the transport properties of these structures. We find that the Hall mobility is an inappropriate measure of the performance of these diamond devices and dramatically overstates the potential device performance.

II. MEASURING THE CONDUCTIVITY OF BORON DELTA-DOPED DIAMOND STRUCTURES

The synthesis of boron delta doped layer structures was carried out using microwave plasma CVD with H_2, CH_4 and B_2H_6 feed gases. Details of the CVD synthesis of delta-doped layers have been reported previously [21]. Synthesis recipes have been developed using both (100) orientated type Ib HPHT single crystal diamond substrates and (100) orientated high purity single crystal CVD diamond substrates. For the Ib substrate, a 0.5 μm intrinsic buffer layer was grown prior to the delta doped layer. For the high purity CVD substrate, the delta-doped layer was deposited directly. A computer-controlled rapid gas switching manifold was used to deposit the delta-doped layers with a thickness of just a few atomic spacing. The delta-doped samples presented in this work were all grown on high purity CVD substrates for which the concentration of background boron and substitutional nitrogen impurities was <0.5 ppb ($<10^{14}$ cm^{-3}) and <5 ppb ($<10^{15}$ cm^{-3}) respectively [22]. Since the delta-layer growth takes place in a different (boron free) reactor from the buffer, we can expect essentially no boron tail on the lower side of the delta layer. Secondary ion mass spectrometry (SIMS) is a powerful analysis tool for assessing delta-doped layers [21] with a dynamic range of 4 – 5 decades giving good sensitivity to impurities such as boron. However, when the delta-doped layer thickness is less than 2.5 nm, the depth resolution of SIMS is compromised by intrinsic broadening due to forward recoil of sputtered ions. In this case we have used

the complementary technique of elastic recoil detection analysis (ERDA) [23] which has reduced dynamic range compared to SIMS but can resolve delta-doped layers with thickness of approximately 1 nm as shown for example in Fig. 1.

The electrical behavior of the delta layers is the most important driver to optimizing the synthesis. As a rapid turnaround tool for guiding synthesis, sheet resistance measurements were employed using the Van der Pauw method with Ag paste contacts applied to the sample corners. For all samples measured electrically, we have opted for a surface delta design rather than a buried delta design with an undoped cap. This avoids the difficulties with achieving Ohmic contacts highlighted previously [20] but increases the effect of interface defects.

Using this technique, the sheet resistance was measured for all samples (i) immediately following CVD which is carried out in a highly reducing atmosphere and therefore it is assumed that the surface is hydrogen terminated, and then (ii) following treatment in a highly oxidizing solution of concentrated H_2SO_4 and KNO_3 at >200°C after which the surface is expected to be oxygen terminated. To support these assumptions, we have carried out contact angle measurements using a Krüss DSA 100 Drop Shape Analyzer and 1 microliter droplets of de-ionized H_2O. We found that the mean contact angle changes from 98° after CVD to 38° following acid treatment corresponding to hydrophobic and hydrophilic behavior associated with hydrogen and oxygen termination of surface dangling bonds respectively.

For decreasing growth time, we observe both a decreasing delta layer thickness and a decreasing peak boron concentration. Fig. 2 shows sheet resistance measurements for a series of delta-doped samples plotted as a function of sheet boron concentration as measured by SIMS. As expected, as the sheet boron concentration decreases (growth time decreases), the sheet resistance increases commensurate with fewer carriers available for conduction. However, for H termination the sheet resistance is inversely proportional to B density whereas it increases much faster for O terminated surfaces. For a sheet boron

concentration of 4.1×10^{13} cm^{-2}, the sheet resistance for H terminated was 91 kΩ/square and when O terminated it increased to 854 kΩ/square. It is understood that this difference is due to interface states which can pin the Fermi level for an O terminated surface 1.7 eV above the valence band maximum [12]. The delta layer is effectively partially compensated and for even thinner delta layers can be completely pinched off. Assuming full activation of the boron and the mobility is unaffected by the surface termination, we have used the sheet resistance and sheet boron concentration to estimate the mobility for the samples in Fig. 2, giving 2–3 cm^2/Vs in all cases. Then using a simple parallel network analysis, this allows a crude estimate of the interface state density associated with the oxygen terminated surface to be made. The estimated interface state density varies from 3.7 to 16×10^{13} cm^{-2} with increasing sheet boron concentration.

In the case of a 1 nm delta layer with boron density of 5×10^{20} cm^{-3} above the metal-insulator transition, the boron atom spacing is comparable to the delta layer thickness, so that lower doped non-metallic samples might involve transport via a 2D rather than a 3D hopping process [24]. However for the lowest sheet density in Fig. 2, and assuming that the delta layer thickness is ~1 nm consistent with Fig. 1, we infer a boron density of 4×10^{20} cm^{-3} suggesting that all these layers have a peak density comparable to, or exceeding, the 3D metal-insulator-transition. This applies even to the oxygen terminated samples despite their lower sheet hole density, since it is the boron concentration which defines the metal-insulator transition density. Hence one might expect the impurity band to be merged into the valence band and metallic behavior to apply to all these samples.

Whilst sheet resistance measurement is a convenient metric to assist growth experiments, in order to detect and measure any enhancement in mobility due to the doped layer being a delta layer, a more sophisticated electrical assessment technique was required such as variable temperature Hall effect.

III. VARIABLE TEMPERATURE HALL MEASUREMENTS

The enhancement in the conductivity of carriers which is expected as a direct result of boron delta doping in diamond compared to conduction through bulk doped material has been predicted from theory to increase the mobility from 1–10 cm^2/Vs to approximately 190 cm^2/Vs [25]. Room temperature Hall measurements on delta-doped structures have previously been reported with Hall mobility values in the range 13–30 cm^2/Vs [17], [26].

Samples from a similar growth series to those plotted in Fig. 2 were fabricated into gated and ungated Hall bars using optical lithography, mesa isolation, and TiPtAu Ohmic contacts. The gate dielectric was Al_2O_3 deposited by atomic layer deposition with thickness between 30 and 64nm, and the gate metal was Al. Mesa-mesa isolation measurements indicated an immeasurably low conductivity of the underlying diamond layer. SIMS measurements were not carried out on these specific samples, however the boron density will be within the range shown in Fig. 2. Variable temperature Hall effect measurements were made between 100 K and 450 K using two systems. First, a polarity-switched DC magnetic field of 5 T at Lake Shore Cryotronics Inc, and secondly a new AC Hall system using a 0.5 T magnet recently developed at the University of Uppsala, were used giving consistent results.

Variable temperature Hall measurements on boron delta-doped diamond have been reported previously [19], but Hall mobility and sheet carrier density was not presented. Fig. 3 shows variable temperature Hall measurements from four representative boron delta-doped samples. Sample 366 had a 20 nm thick heavily boron doped layer and shows comparatively weak temperature dependence. This is in contrast to recent Hall measurements of heavily doped bulk diamond which found strong temperature dependent behavior [27]. It appears that our bulk material shows true metallic behavior. However, our thin delta layer samples exhibit a number of important but common temperature dependent features which have allowed us to gain a new understanding of transport in delta-doped structures. For instance at low

temperature, the measured Hall mobility is very low (~1 cm^2/Vs), then increases with increasing temperature, then plateaus and even begins to drop again at the highest temperature range. These observations at first sight are surprising as generally the mobility of carriers in a semiconductor crystal decreases with increasing temperature due to an increase in the phonon scattering rates. The highest measured Hall mobility was 900 cm^2/Vs at room temperature.

Gated Hall measurements were performed on sample 506 which had sufficiently low carrier density that it could be pinched-off with a gate voltage of 30V across the 63nm thick Al_2O_3 dielectric. Hall measurements were taken as a function of applied gate voltage up to 30 V and between 200K and 350K and are shown in Fig. 4. Fig. 4(a) shows the sheet hole density and sheet conductivity dependence with gate voltage. As the gate voltage is increased, the conductivity decreases as the delta layer is depleted. The hole density can only be pinched off at low temperatures with a very soft turn-off observed. Fig. 4(b) is a plot of measured Hall mobility as a function of gate voltage. Interestingly at each temperature, as the delta layer is depleted and the sheet conductivity falls dramatically, we observe that the Hall mobility remains relatively constant. At each fixed gate voltage, a similar temperature dependent behavior to that seen in Fig. 3 is observed, but within the same sample.

IV. MULTI-CARRIER MODEL

To help us interpret the temperature dependencies shown in Figs. 3 and 4, we have developed a model of conduction in delta-doped structures which considers carriers with different mobility and number density. We note that conduction in parallel channels in delta layers was first invoked to explain impedance spectroscopy results [18].

We propose a model which describes thermal activation of holes from the delta-doped layer into bulk states within the intrinsic buffer where there is reduced scattering from ionized boron acceptors [25]. An

alternative interpretation is that there is excitation of holes from the ground state subband of the delta-function potential well into higher subbands in the valence band with higher mobility [28]. However, it is apparent that there is no simple division between states localized in the delta layer and those forming the bulk of the diamond. Hence in order to correctly describe the measured Hall mobility, a multi-carrier model rather than a simple homogeneous single layer transport approach is required. Here conduction occurs in N adjacent layers, or alternatively N subbands co-located within the same region. The first (classical) interpretation holds if carriers can be considered to be strongly localized within specific layers. The latter interpretation is valid in a 2D quantum well assuming that interband scattering rates are much smaller than intraband scattering rates. The Hall mobility in the multi carrier model is given by [29]:

$$\mu_H = \sum_{i=1}^{N} p_{si}\mu_i^2 \Big/ \sum_{i=1}^{N} p_{si}\mu_i \tag{1}$$

To have as simple as possible a model that can reasonably well describe the data and limit the number of fitting parameters, we have used a two carrier-type model (we will relax this assumption in section VI). In this case, the Hall mobility represented in (1) simplifies to:

$$\mu_H = \left(p_{s1}\mu_1^{\,2} + p_{s2}\mu_2^{\,2}\right)/\left(p_{s1}\mu_1 + p_{s2}\mu_2\right) \tag{2}$$

The measured Hall mobility for a two carrier-type model is a function of the mobility and sheet number density of each individual layer (or subband) (2). Furthermore, the apparent sheet carrier density is given by the expression [29]:

$$p_{s,app} = \left(p_{s1}\mu_1 + p_{s2}\mu_2\right)^2 /\left(p_{s1}\mu_1^{\,2} + p_{s2}\mu_2^{\,2}\right) \tag{3}$$

The interpretation that agrees with experimental data is that holes in the lowest energy state have sheet density p_{s1} and mobility μ_1, and as the temperature increases, holes with density p_{s2} and mobility μ_2 are excited into either bulk states in the buffer layer or higher energy confined subbands. The number of

carriers thermally excited can be calculated from the integral over all energy *E* of the 3D density of states which has an $E^{1/2}$ dependence, multiplied by the probability that these states are occupied (i.e. the Fermi-Dirac probability distribution function). This gives:

$$p_{sheet}^{Bulk} \sim T^{3/2} \exp\left[(E_F - E_V)/k_B T\right] \tag{4}$$

Equation (4) predicts a $T^{3/2}$ and a *exp(E/kT)* dependence. We have implemented this two-carrier type model using (4) combined with expressions describing the temperature dependent mobility. In a doped semiconductor, a $T^{3/2}$ dependence normally applies to impurity scattering in extended states. However, from our own observations (Fig. 4(b)), and the work from other groups [27], it is clear that predicting the temperature dependence for heavily boron doped diamond is non-trivial. Therefore, in the heavily doped type 1 region we have described the mobility using an empirical function (5) containing a $T^{2/3}$ dependence where $\mu_{1,0}$ is a free fitting parameter.

$$\mu_1(T) = \mu_{1,0}\left(T/300K\right)^{2/3} \tag{5}$$

For the lightly doped type 2 region, the mobility from interaction with acoustic and optical phonons is described by an empirical function containing a $T^{-3/2}$ dependence where $\mu_{2,0}$ is a free fitting parameter (6), and an empirical relationship (7) resulting from a fit to time of flight measurements of hole mobility for bulk high purity CVD diamond [30] respectively, which are combined by applying the Matthiessen rule (8).

$$\mu_{2,ac}(T) = \mu_{2,0}\left(T/300K\right)^{-3/2} \tag{6}$$

$$\mu_{2,op}(T) = 1.786\times10^{5}\exp\left(-1.13\times10^{-2}T\right) \tag{7}$$

$$\mu_2(T) = \left[\left(1/\mu_{2,ac}\right)+\left(1/\mu_{2,op}\right)\right]^{-1} \tag{8}$$

The resulting two-carrier type model has been manually fitted to experimental Hall data, for example as shown for sample 459 in Fig. 5. This two-carrier type model reproduces successfully the observed

behavior of the sheet hole concentration, Fig. 5(a) and the Hall mobility, Fig. 5(b). The apparent drop in sheet hole density with increasing temperature is due to the thermal re-distribution of carriers between the two types, and the actual total number density of holes remains constant throughout the temperature range. In the case of sample 459, the total carrier density was determined to be 1.9×10^{13} cm^{-2}. The model predicts that at room temperature the concentration of carrier type 1 is >99.9%, as indicated in Fig. 5(b) inset i.e. less than 0.1% of carriers have been thermally promoted to the higher mobility carrier type 2. For samples 348 and 459, the values of activation energy (E_F-E_V) determined by the model were 0.25 eV and 0.21 eV respectively. For sample 506, the activation energy did not vary strongly with gate bias and showed energies of 0.18 eV, 0.18 eV, and 0.17 eV at 0 V, 15 V, and 30 V respectively. We will return to the physical interpretation of this energy in section VI.

V. CONDUCTIVITY MOBILITY

We need to reconcile the apparently high room temperature Hall mobility (440 cm^2/Vs for sample 459) with the very high sheet resistance (126 kΩ/square for sample 459) which implies a mobility of 2-3 cm^2/Vs. This difference arises because the conductivity results from a linear combination of the mobility in the two regions as in (9) below, rather than from the combination of squares that applies to the Hall effect (2).

$$\mu_{conductivity} = \left(p_{s1}\mu_1 + p_{s2}\mu_2\right)/\left(p_{s1} + p_{s2}\right) \tag{9}$$

In an example plot of mobility calculated using (2) and (9) as a function of carrier type 2 occupation as shown in Fig. 6, we observe that when $\mu_2 >> \mu_1$ this results in a much higher value for μ_H than $\mu_{conductivity}$ even when carrier type 2 occupation is small. Indeed μ_H is always greater than $\mu_{conductivity}$. In the context of the two carrier-type model, it can be seen that μ_H increases very rapidly as carriers are transferred from the low to high mobility region, while the conductivity mobility only increases linearly.

Using the two carrier-type model, the conductivity mobility was calculated as a function of temperature for each sample. As shown in Fig. 5 for Sample 459, the conductivity mobility (~1.0 cm^2/Vs) is significantly lower than the measured Hall mobility (440 cm^2/Vs) at room temperature because the percentage of thermally promoted carriers is small (0.1%). The room temperature conductivity mobility determined for all samples was in the range 1 – 4 cm^2/Vs. Hence one can conclude that for delta-doped structures, simple Hall mobility measurements give an over-estimate of the conductivity of the sample, and do not give an appropriate representation of the material performance. This fully explains the observation of high sheet resistance on samples with high measured Hall mobility. Using the two-carrier model, one can demonstrate that between 20% and 30% of carriers thermally promoted to the higher mobility type are required to achieve a value of conductivity mobility significantly above 100 cm^2/Vs, whereas experimentally we observe a typical room temperature value closer to 0.1%.

In support of this interpretation, we have collected 3-terminal I-V data from fabricated long channel FETs and gated Hall bars. Specifically, the gate transfer characteristics were analyzed and the *field-effect* mobility was extracted from the transconductance and gate capacitance using (10), where L_g and W_g are the gate length and width, C_{ox} is the Al_2O_3 capacitance, g_m is the peak transconductance, and V_{DS} is the voltage drop under the gate [29].

$$\mu_{FE} = L_g g_m / \left(W_g C_{ox} V_{DS} \right) \tag{10}$$

For sample 459, a figure for the field-effect mobility of 1.9 cm^2/Vs was measured. For all samples, the room temperature field-effect mobility varied between 0.2 – 2 cm^2/Vs, in reasonable agreement with the conductivity mobility extracted from the two carrier-type model analysis. This observation suggests that the charge in the delta layer is directly modulated by the gate and the delta layer charge is not screened from the gate by the interface state charge i.e. the occupation of the interface states is not changed by the gate bias. The consistency between the conductivity mobility extracted by analysis of the Hall data and

the field-effect mobility suggests strongly that all the carriers in the low energy state act as a 2D hole gas and are equally affected by the gate bias. Hence any MESFET-like interpretation within the delta layer in terms of a gate voltage dependent depletion layer thickness must be incorrect.

VI. Discussion and Physical Model

The two-level model presented in section IV is somewhat phenomenological in nature, so here we attempt to provide a more physical basis for the observations. It seems highly likely that the high mobility channel corresponds to hole transport in extended valence band states and we will make this assumption. However the physical origin of the low mobility channel is less clear. The observations are that (i) the low mobility channel shows a mobility which is temperature dependent and appears to decrease as the hole density falls, (ii) the boron volumetric density in the delta layer is comparable to the metal-insulator-transition density with a sheet boron density exceeding 10^{13}cm^{-2} in all cases, (iii) the hole sheet density can be as much as a factor of 10^4 lower than the boron sheet density as a result of oxygen termination, (iv) the two carrier-type model suggests an activation energy between the channels of around 0.2eV.

Here are some possibilities for the origin of the delta layer related low mobility channel observed at low temperature, with activation to extended states in the valence band being responsible for the high mobility channel:

1. Hopping occurs between oxygen related interface states ~1.7eV above the valence band.
2. The boron density in the delta layer is below the metal-insulator-transition density and hopping occurs within a separate boron impurity band.
3. The boron density in the delta layer is above the metal-insulator-transition density, but hopping occurs within band tail states within the delta layer.
4. Metallic conduction occurs in the valence band within the delta layer.

The temperature dependence does appear to suggest that the transport is occurring by a mechanism such as hopping [31] and is not simply metallic conduction within the delta layer. We can reject hopping between interface states since these are energetically much too high above the valence band. Impurity band hopping conduction could explain the activation energy and the temperature dependent conduction, but the observation of 99.99% compensation of the boron by the interface states would require another mechanism to achieve this precise charge balance. However, this apparent precise charge compensation could be explained if most of the holes were localized in disorder induced band tail states [32] either within the tails of an impurity band or the valence band edge. The high concentration of boron would induce disorder, with the occupation probability of the acceptors being reduced by compensation by interface states. Only a small proportion of those remaining holes would be available for conduction since most would be localized. There has been considerable discussion of the effect of heavy boron doping on the band structure [33], but the consensus appears to be that the boron impurity band merges with the valence band, and contrary to [27], our measurements of bulk material shown in Fig. 3 appear to be consistent with that picture. Our delta layers all have a density comparable to the 3D metal-insulator transition so we believe the most likely explanation is that the hopping occurs in band tail states, but an impurity band is still quite possible.

To see how the delta-layer subband structure would affect the transport in such a model, and neglecting any localization induced band-tailing, we have undertaken a 1D Schrödinger-Poisson simulation of the device structure using Silvaco ATLAS software. This calculates the energies for the heavy, light and split-off hole subbands assuming that the boron is fully activated (i.e. the impurity band is located within the valence band). Fig. 7(a) shows the subband energies for an example structure. The delta-well is a narrow well inside a confining triangular potential well which results from the depletion field from ionized residual deep donors. Note that a confining potential is essential for FET device operation since it prevents buffer leakage and suppresses short-channel effects [34]. As can be seen from Fig 7(b), the 2D subbands form a finer and finer comb the higher the hole energy, eventually merging into a 3D band.

Let us first consider the expected mobility for the ground state which, as we can see from Fig. 7(c), is where most holes will be found. We have developed a best-case simple model for the mobility based upon relaxation time theory and an application of Fermi's golden rule. The standard expression for the mobility of a hole in a semiconductor is [35]:

$$\mu = e < \tau > / m^* \tag{11}$$

where e is the charge of the hole, m^* is the effective mass and $<\tau>$ is the average hole lifetime between scattering events. To simplify the model, we have assumed for the delta-doped structure, that carrier scattering is dominated by ionized impurities (boron). The contribution from neutral impurities, phonon interactions, surface roughness and carrier-carrier collisions are treated as a constant value and are calculated using the value for the mobility of holes in bulk diamond. The ground state hole wavefunction is described using the Fang-Howard wavefunction [36]. This describes the hole as a non-local entity and has a probabilistic distribution across the doped and undoped regions. We apply the standard model for calculating the mobility of hole bands in a delta layer [37] which takes into account screening effects. Thus the expression for the relaxation rate of holes scattering from ionized impurities in the delta layer is given as:

$$\tau^{-1} = \left(4\pi^2 / h\right)\int dz N(z) \times \sum_q \left[\left[2\pi e^2 / q\varepsilon(q)\right] F(q,z)\right|^2 (1-\cos\theta)\delta\left(\varepsilon_k - \varepsilon_{k-q}\right)\Big] \tag{12}$$

where h is Planck's constant, $N(z)$ is the doping profile, q is the 2D wave vector of the hole, $\varepsilon(q)$ is the static dielectric screening function, $|F(q,z)|^2$ is the hole overlap integral (dependent on the hole location), θ is the angle between the incident and the scattered hole, and ε_k is the energy of the hole with wave vector k. From (12), and applying Matthiessen's rule to include the bulk scattering rate, we calculate the total relaxation rate at room temperature and hence the total mobility for the holes in the subband.

Calculations for typical delta doped structures (i.e. B_{peak} =1×10^{20} cm^{-3} and thickness 1 nm) and where all holes are confined to the delta layer, give a lower limit to the value of total mobility of 2.9 cm^2/Vs. Estimating an upper limit can be done by taking an extreme case where the wavefunction is expanded such that less than 10% of the holes are located within the delta layer resulting in <40 cm^2/Vs. In our study, we have used oxygen terminated samples and surface delta layers so we can expect that charge depletion by interface states and surface roughness will reduce mobility somewhat below these theoretical predictions. Nevertheless there does seem to be reasonable agreement with the measured mobility of around 2 cm^2/Vs. We note that for a 1 nm delta layer, the upper limit of mobility in the ground state is significantly smaller than the mobility enhancement of up to 190 cm^2/Vs originally predicted in [25].

Let us now estimate the Hall and conductivity mobility which would result from summing over all available subbands using the Schrödinger-Poisson simulation. We make the assumption that the intersubband scattering rate is much longer than the intrasubband rate, and we simplify Matthiessen rule such that the scattering rate is given by:

$$\frac{1}{\tau_{avg}} = \int_0^d \frac{1}{\Omega_i} |\psi(z)|^2 dz + \int_0^\infty \frac{1}{\Omega_B} |\psi(z)|^2 dz \qquad (13)$$

where $\psi(z)$ is the wave function associated with each sub-band and d is the delta layer thickness. This empirical relationship represents the appropriate weighting for transport mechanisms from the bulk and the delta layer for each mode taking influence from Eq. (12). As such, the first term is a simplified form of Eq. (12) and the second term represents the bulk diamond scattering mechanisms. To be consistent with our treatment of the mobility temperature dependence in section IV, in Fig. 7 we have assumed that Ω_i=14.5×(T/300)$^{2/3}$ ps and Ω_B=5×(T/300)$^{-3/2}$ ns. This gives a heavy-hole mobility of 2.9 cm^2/Vs at 300 K for an electron confined inside the delta layer and a heavy-hole mobility of 1000 cm^2/Vs at 300 K when the delta layer is not present. This process results in a mobility in each subband which is plotted in Fig. 7(d) and indicates that the hole mobility rapidly increases as the energy drops below the valence band

maximum. This approach is consistent with previous studies on delta layers [36] and lends support to a metallic conduction.

We can now use the subband occupancy to integrate (1) and the multi-band version of (9) to evaluate Hall and conductivity mobility. These integrals weight each subband by either the subband mobility, or the mobility squared, and result in the energy dependent contributions to mobility shown in Figs. 7(d) and (e). It is very instructive to note that the conductivity mobility is clearly weighted towards the low mobility ground state, whereas the Hall mobility is weighted towards states located about 0.2 eV below the valence band edge with much higher mobility.

Fig. 8 shows how the calculated Hall parameters (mobility and number density) vary as a function of temperature. It can be seen that the key trends shown in Figs. 3 and 4 have been accurately captured by this model. Activation from the low mobility states in the delta layer potential-well to more extended states results in a rapid increase in Hall mobility with increasing temperature and a much slower increase in conductivity mobility. This detailed Schrödinger-Poisson based model is consistent with the two-carrier type model of section IV. If we use the two-carrier type model to fit the data of Fig. 8, we find an activation energy between the two levels of 0.17 eV in good agreement with experiment. Varying the thickness of the delta layer between 1 and 3 nm and the boron concentration between 10^{20} and 5×10^{20} cm^{-3} all gave similar activation energy consistent with the experimental observations shown in Fig. 3.

VII. CONCLUSION

In this paper, we have described the development of boron delta-doped CVD diamond structures. We have demonstrated surface delta layers with thicknesses of order 1 nm which are substantially compensated by an oxygen terminated surface. Sheet resistance measurements failed to detect the conductivity enhancement expected for delta layers of this thickness. However detailed variable temperature Hall effect measurements obtained values of Hall mobility up to 900 cm^2/Vs. A key finding

and new understanding from this work is that the standard treatment of Hall measurements using a single homogeneously doped layer results in a dramatic over-estimate of the performance of the delta layer. Indeed, we have shown that despite the high values of Hall mobility, the room temperature conductivity mobility is actually in the range 1 – 4 cm^2/Vs for all samples measured, and it is the conductivity mobility which is important for most device applications. Measurements of the field-effect mobility extracted from the gate characteristics of FET devices were in close agreement with the conductivity mobility.

We have shown that a physical model based on activation from states largely residing within localized states within a highly doped delta layer to more extended states in the bulk of the diamond can fully explain the observed temperature dependence of the Hall and conductivity mobility. This has shown that the vast majority of carriers remain confined within the delta layer where ionized impurity scattering results in low mobility. A simple two-carrier version of the model allows rapid analysis of the data, and has shown that even a small fraction of carriers thermally promoted to a higher mobility carrier type has a dramatic effect on the measured Hall mobility but without impacting the conductivity mobility. Finally, we have developed a scattering model which predicts that the mobility of holes in the ground state, where most holes reside, will yield a room temperature mobility of <40 cm^2/Vs even for the most optimistic scenario.

A very recent letter published while this paper was in review also reports temperature dependent Hall mobility in delta doped boron diamond which they also explain as a two channel conduction process [38]. It is argued that the high mobility channel is associated with conduction in the buffer associated with residual boron. In our case, we can be quite certain that the high mobility conduction process is not associated with the bulk of the buffer since we observe no conduction in mesa isolation structures.

The results and conclusions presented here apply specifically to surface delta layers. It is expected that a degree of improvement of the mobility of carriers in a buried delta layer will be achieved due to the

greater opportunity for carrier transport in undoped regions, and a reduced compensation by oxygen related interface states, however this improvement will be limited when the top cap layer is depleted by the gate field during transistor operation.

The evidence from this work strongly indicates that to achieve a high conductivity mobility in a boron delta-doped CVD diamond structure and therefore achieve the high frequency and high current carrying performance that is required from a practical diamond transistor, a high degree of carrier excitation is required from the lowest subband into 3D bulk states. The challenge is to achieve this at room temperature.

ACKNOWLEDGMENT

The authors would like to thank Prof Sir Christopher Snowden from the University of Surrey and Prof Peter Houston from the University of Sheffield for valuable guidance and conversations and Dr Kean-Boon Lee from the University of Sheffield for FET characterization. This work was funded by Diamond Microwave Devices Ltd, the Defence Science and Technology Laboratories and the UK Technology Strategy Board. JI and SM also wish to thank the Swedish Research Council for financial support.

REFERENCES

[1] S. Barman, and G.P. Srivastava, J. Appl. Phys. **101**, 123507, (2007).

[2] C.A. Klein, and R. DeSalvo, Applied Physics Letters, **63**, 1895, (1993).

[3] P. Liu, R. Yen, and N. Bloembergen, IEEE Journal of Quantum Electronics, **14**, 574, (1978).

[4] J. Isberg, J. Hammersberg, E. Johansson, T. Wikstrom, D.J. Twitchen, D. J., A.J. Whitehead, S.E. Coe, and G.A. Scarsbrook, Science **297**, 1670, (2002).

[5] A. Aleksov, A. Denisenko, U. Spitzberg, W. Ebert, and E. Kohn, IEEE Electron Device Letters, **23**, 488, (2002).

[6] H. Umezawa, K. Hirama, T. Arai, H. Hata, H. Takayanagi, T. Koshiba, K. Yohara, S. Mejima, M. Satoh, K-S. Song, and H. Kawarada, Japanese Journal of Applied Physics, **44**, 7789, (2005).

[7] K. Ueda, Y. Yamauchi, T. Makimoto, M. Schwitters, D.J. Twitchen, G.A. Scarsbrook, and S.E. Coe, IEEE Electron Device Letters **27**, 570, (2006).

[8] K. Hirama, T. Koshiba, K. Yohara, H. Takayanagi, S. Yamauchi, M. Satoh, and H. Kawarada, 18th International Symposium on Power Semiconductor Devices & IC's Naples, Italy, p. 69, (2006).

[9] M. Kasu, K. Ueda, Y. Yamauchi, A. Tallaire, and T. Makimoto, Diamond & Related Materials, **16**, 1010, (2007).

[10] K. Shinohara, D. Regan, I. Milosavljevic, A.L. Corrion, D.F. Brown, P.J. Willadsen, C. Butler, A. Schmitz, S. Kim, V. Lee, A. Ohoka, P.M. Asbeck, and M. Micovic, IEEE Electron Device Letters. **8**, 1074, (2011).

[11] Y.-F Wu, M. Moore, A. Saxler, T.Wisleder, and P. Parikh, 64th Device Research Conference, Pennsylvania, US, p. 151, (2006).

[12] A. Denisenko, C. Pietzka, A. Romanyuk, H. El-Hajj, and E. Kohn, Journal of Applied Physics **103**, 014904, (2008).

[13] E. F. Schubert, Delta-doping of semiconductors . Cambridge University Press, (1996), pp. 487-497.

[14] T. Klein, P. Achatz, J. Kacmarcik, C. Marcenat, F. Gustafsson, J. Marcus, E. Bustarret, J. Pernot, F. Omnes, Bo E. Sernelius, C. Persson, A. Ferreira da Silva, and C. Cytermann, Physical Review B **75,** 165313 (2007).

[15] A. Kawano, H. Ishiwata, S. Iriyama, R. Okada, T. Yamaguchi, Y. Takano and H. Kawarada, Physical Review B **82**, 058318 (2010).

[16] J.-P. Lagrange, A. Deneuville, and E. Gheeraert, Carbon, **37**, 807, (1999).

[17] R. Edgington, S. Sato, Y. Ishiyama, R. Morris, R.B. Jackman and H. Kawarada, Journal of Applied Physics **111**, 033710 (2012).

[18] N. Tumilty, J. Welch, R. Lang, C. Wort, R.S. Balmer, and R. Jackman, Journal of Applied Physics, **106**, 103707, (2009).

[19] M. Kunze, A. Vescan, G. Dollinger, A. Bergmaier, and E. Kohn, Carbon, **37**, 787, (1999).

[20] H. El-Hajj, A. Denisenko, A. Kaiser, R.S. Balmer, and E. Kohn, Diamond & Related Materials, **17**, 1259, (2008).

[21] R.S. Balmer, I. Friel, S.M. Woollard, C.J.H. Wort, G.A. Scarsbrook, S.E. Coe, E. El-Hajj, A. Kaiser, A. Denisenko, E. Kohn, and J. Isberg, Philosophical Transactions of the Royal Society A, **366**, 251, (2008).

[22] R.S. Balmer, J.R. Brandon, S.L. Clewes, H.K. Dhillon, J.M. Dodson, I. Friel, P.N. Inglis, T.D. Madgwick, M.L. Markham, T.P. Mollart, N. Perkins, G.A. Scarsbrook, D.J. Twitchen, A.J. Whitehead, J.J. Wilman and S.M Woollard, Journal of Physics: Condensed Matter **21** 364221 (2009).

[23] G. Dollinger, A. Bergmaier, L. Goergens, P. Neumaier, W. Vandervorst, and S. Jakschik, Nucl. Instrum. Methods B, **219-220**, 333, (2004).

[24] T. Ando, A. B. Fowler, and F. Stern, Reviews of Modern Physics **54**, pp. 437-672, (1982).

[25] E. Kohn and A. Denisenko, "Doped diamond electron devices" Ch14 in "CVD Diamond for electronic devices and sensors", Ed. R.Sussman, Wiley, pp. 320-321, (2009).

[26] H. El-Hajj, A. Denisenko, A. Bergmaier, G. Dollinger, M. Kubovic, and E. Kohn, NDNC 2007 Proceedings of the International Conference on New Diamond and Nano Carbons 2007, Diamond & Related Materials, **17**, 409, (2008).

[27] M. Aono, O. Maida, and T. Ito, Diamond & Related Materials, **20**, 1357, (2011).

[28] J.H. Davies, The Physics of Low Dimensional Semiconductors. Cambridge, UK: Cambridge University Press, (1997).

[29] D.K. Schroder, "Mobility." in D. K. Schroder, Semiconductor Material and Device Characterization, 3rd Ed. New Jersey: IEEE Press, Wiley Inter-Science. pp. 465-522. (2006).

[30] M. Gabrysch, S. Majdi, D.J. Twitchen, and J. Isberg, Journal of Applied Physics, **109**, 063719, (2011).

[31] T.H. Borst and O.Weis, Physica Status Solidi (a), **154**, 423, (1996).

[32] N.F. Mott, Metal-Insulator Transitions, 2nd Ed., Taylor and Francis, (1990).

[33] J.P. Goss, R.J. Eyre, and P.R. Briddon, Physica Status Solidi (b), **245**, 1679, (2008).

[34] R.H. Dennard, F.H. Gaensslen, H-N. Yu, V.L. Rideout, E. Bassous, and A.R. LeBlanc, IEEE Journal of Solid-State Circuits, **SC-9**, 256, (1974).

[35] P.Y. Yu, and M. Cardona, Fundamentals of Semiconductors. Berlin, New York: Springer-Verlag, (2001).

[36] F.F. Fang, and W.E. Howard, Physical Review Letters, **16**, 797, (1966).

[37] E.F. Schubert, Delta-doping of semiconductors . Cambridge University Press, p. 392, (1996).

[38] G. Chicot, T. N. Tran Thi, A. Fiori, F. Jomard, E. Gheeraert, E. Bustarret, and J. Pernot, Applied Physics Letters **101**, 162101 (2012).

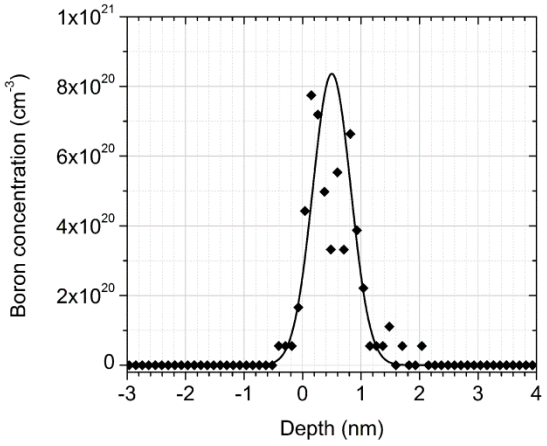

Fig. 1. A plot of the boron profile of an example delta layer measured by ERDA showing a full width at half maximum of 1 nm. Solid line represents a Gaussian fit to the measured data, the boron from depth < 0 nm is a measurement artifact.

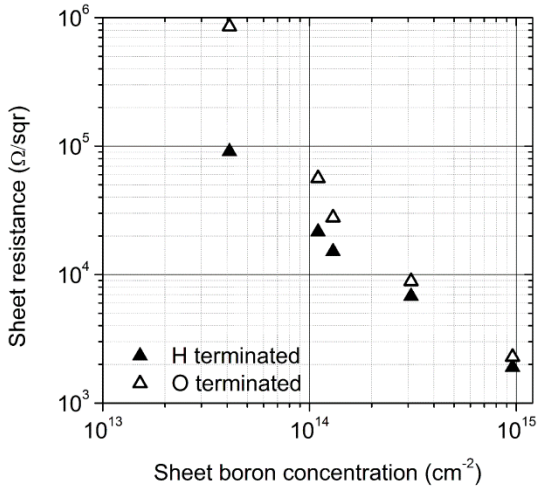

Fig. 2. Sheet resistance as a function of sheet boron concentration for delta-doped layers with hydrogen and oxygen terminated surfaces from a systematic study.

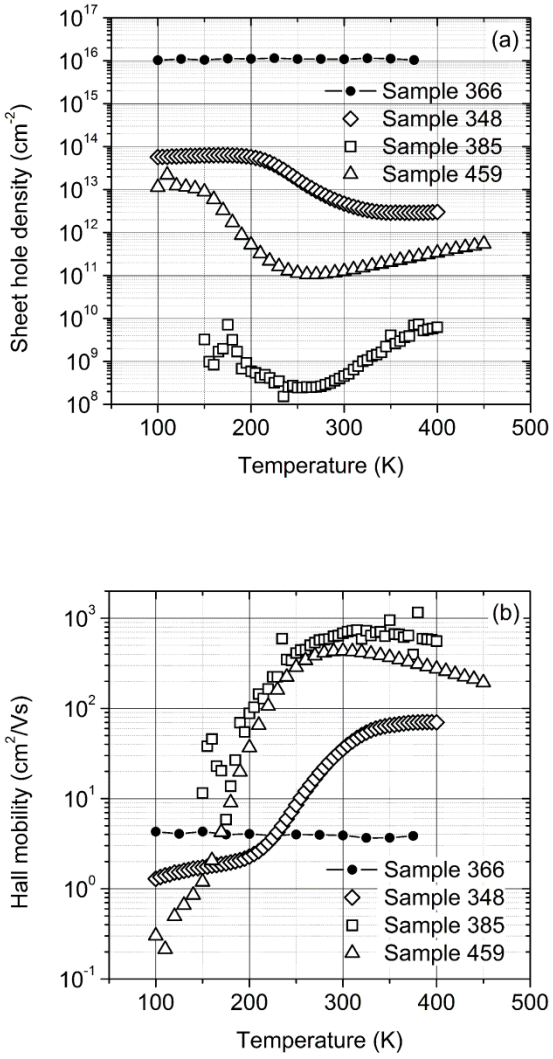

Fig. 3. Variable temperature Hall Effect measurements using a Hall bar configuration for 4 samples with different delta thicknesses: (a) sheet hole density, and (b) Hall mobility.

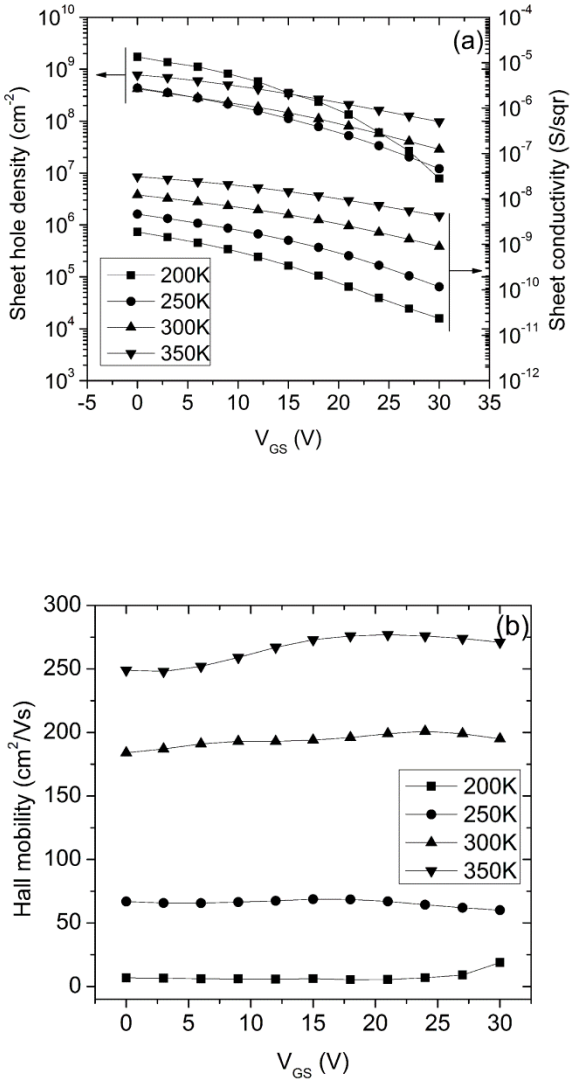

Fig. 4. Gated Hall measurements from sample 506. (a) Sheet hole density and sheet conductivity and (b) Hall mobility as a function of gate voltage.

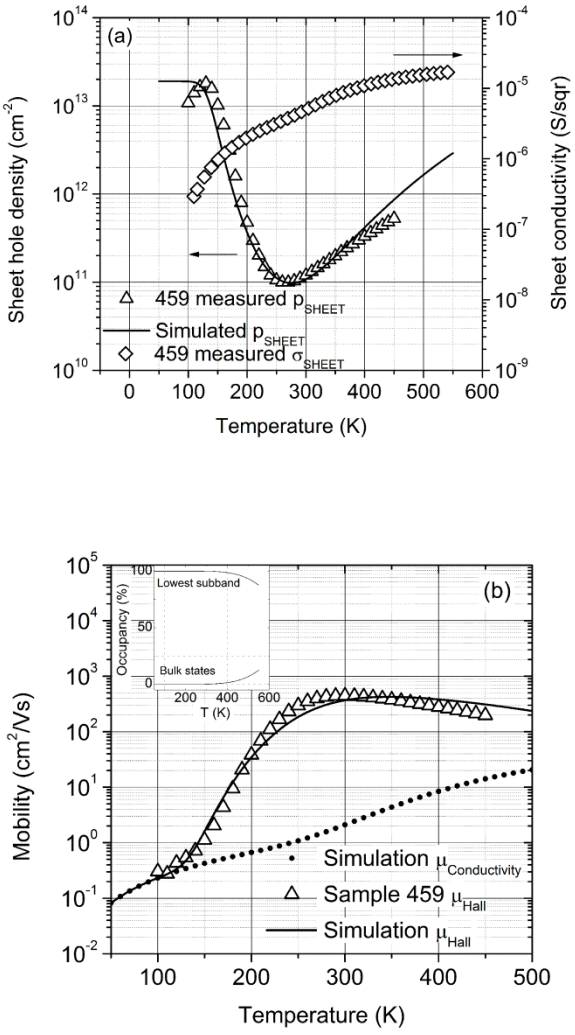

Fig. 5. Temperature dependent measurements of sample 459. Note that the data shown here is a repeat measurement on a different Hall bar structure to that shown in Fig. 3 demonstrating reproducibility. (a) measured sheet hole density and sheet resistance, and simulated sheet hole density using two-carrier type model. (b) measured Hall mobility and simulated Hall mobility using two-carrier type model. Also plotted is the conductivity mobility extracted using the two-carrier type model. Inset is a plot of percentage carrier occupancy in the lowest subband and bulk states.

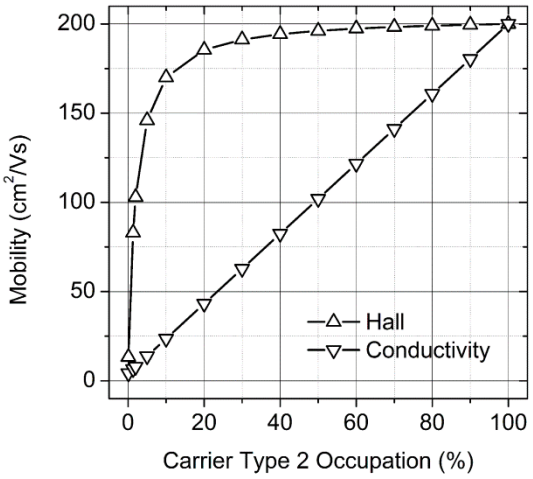

Fig. 6. Hall mobility and conductivity mobility as a function of carrier type 2 occupation for a typical set of parameters: μ_1 = 4 cm^2/Vs, μ_2 = 200 cm^2/Vs and $p_{s1} + p_{s2} = 10^{13}$ cm^{-2}.

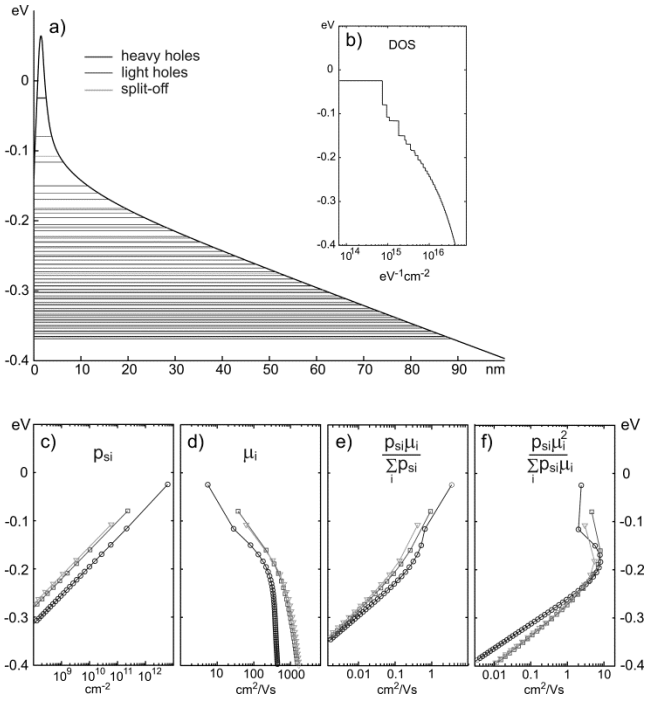

Fig. 7. A room temperature simulation using Silvaco ATLAS of a delta layer structure with 60 nm Al_2O_3, 1 nm delta layer with boron density 10^{20} cm^{-3}, and bulk nitrogen density 10^{14} cm^{-3}. The boundary conditions are: equal potential at a contact on the Al_2O_3 surface (not shown in the figure) and on the diamond back surface. Wavefunctions are assumed to vanish outside the diamond. (a) Potential well and maximum energy for the first 60 heavy, light and split-off hole subbands. The x-axis denotes distance in nanometers into the diamond with the origin at the Al_2O_3-diamond interface. The origin of the y-axis is at the Fermi level which is 2.70 eV below the surface contact potential. (b) Density of states, (c) hole occupation, (d) drift mobility, (e) weighted conductivity mobility, (f) weighted Hall mobility, in each subband *i*. For (c-f) circles, squares and triangles mark heavy, light and split-off hole subbands, respectively.

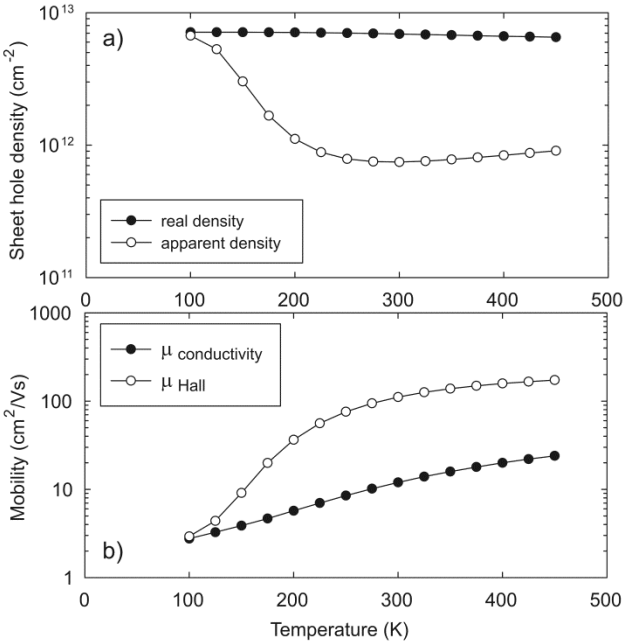

Fig. 8. Temperature dependence of the simulated Hall mobility and number density using the same structure as in Fig. 7.